2010-2012 EQC project "Electrical conductivity structure of the Alpine Fault and its relationship to seismicity and seismogenesis"

T. Grant Caldwell[1], Stephen Bannister[1], Sandra Bourguignon[1], Graham J. Hill[1], Edward A. Bertrand[1], Stewart L. Bennie[1], Wiebke Heise[1], Yasuo Ogawa[2] and Hugh M. Bibby[1]

1. GNS Science, Lower Hutt
2. Tokyo Institute of Technology

CONTENTS

FIGURES

Layman's Summary

The occurrence time of an earthquake on a fault ultimately depends upon the build-up of stress on the fault overcoming the strength of the frictional force resisting the fault rupturing. Since we are unable to measure these forces directly, we must use surface geophysical measurements to provide information about other properties that are indirectly related to these forces. In this EQC funded project we have used information gathered from an array of seismometers and from measurements of natural fluctuations in the Earth's magnetic field to study a 50 km long segment of the Alpine Fault on the west coast of the South Island. From this information we have been able to determine the depth at which rocks close to the Alpine Fault become too soft or ductile to allow micro-earthquakes to occur to creep in response to plate-tectonic forces driving the fault. The depth at which the rocks become ductile is one of the key factors that will control the ultimate size of a future Alpine Fault earthquake. We have also shown that the rocks are electrically conductive in the ductile region beneath the fault. The high conductivity indicates that high pressure fluids are present in the fault's root zone. These fluids will reduce the frictional strength above, especially if they leak upwards. Comparison with other measurements 40 km further to the south show that the electrical conductivity structure there is different, perhaps reflecting a change in the frictional strength of the fault. Our work provides a glimpse into the inner workings of the Alpine Fault that will help us better understand the hazard it poses.

Technical Abstract

We have collected and analysed new magnetotelluric (MT) data and determined the 3-D distribution of seismicity and seismic properties from a ~60 km long segment of the Alpine Fault between Whataroa and Ross. MT data from 85 new measurements sites show that a south-eastward dipping electrically-conductive zone is present in the mid-crust about 10 km south-east of the Alpine Fault, in good agreement with the conductivity structure inferred from an earlier MT survey along the Whataroa. This structure is interpreted to be a ductile shear zone at the down-dip extension of the Alpine Fault below the frictionally locked part of the fault. The conductive zone continues northwards to at least Ross; the high electrical conductivity indicating the presence of (electrically) interconnected fluid within the inferred shear zone.

Earthquake seismic data recorded by the GeoNet network and two temporary seismometer arrays: ALFA08 and ALFA09 provide complementary information on the seismicity distribution and seismic properties of the crust from the northern part this segment of the fault, between Harihari and Ross. Double-difference analysis of the seismological data using a detailed 3-D velocity model was used to relocate 1062 earthquakes concentrated southeast of this part of the fault. The relocated seismicity shows that more than 70% of the events are concentrated in a 12 km wide band centred 16 km southeast of the fault. Almost all of the earthquakes shallower than ~4 km occur within this band. Ninety five per cent of the seismicity occurs above 8 km and this depth limit does not appear to change significantly with distance south-east of the fault. If we assume that the 95% depth limit of seismicity can be identified with the transition to ductile behaviour and that this depth is controlled by temperature alone, our results suggest that the thermal structure southeast of this part of the doesn't vary significantly with distance from the fault.

Introduction

Here we report the results of a magnetotelluric (MT) survey and seismological data for the segment of the Alpine Fault between Whataroa and Ross (Figure 1). Funding from EQC supported the helicopter borne part of the MT data collection and the analysis of seismological data collected previously by GNS in the same region.

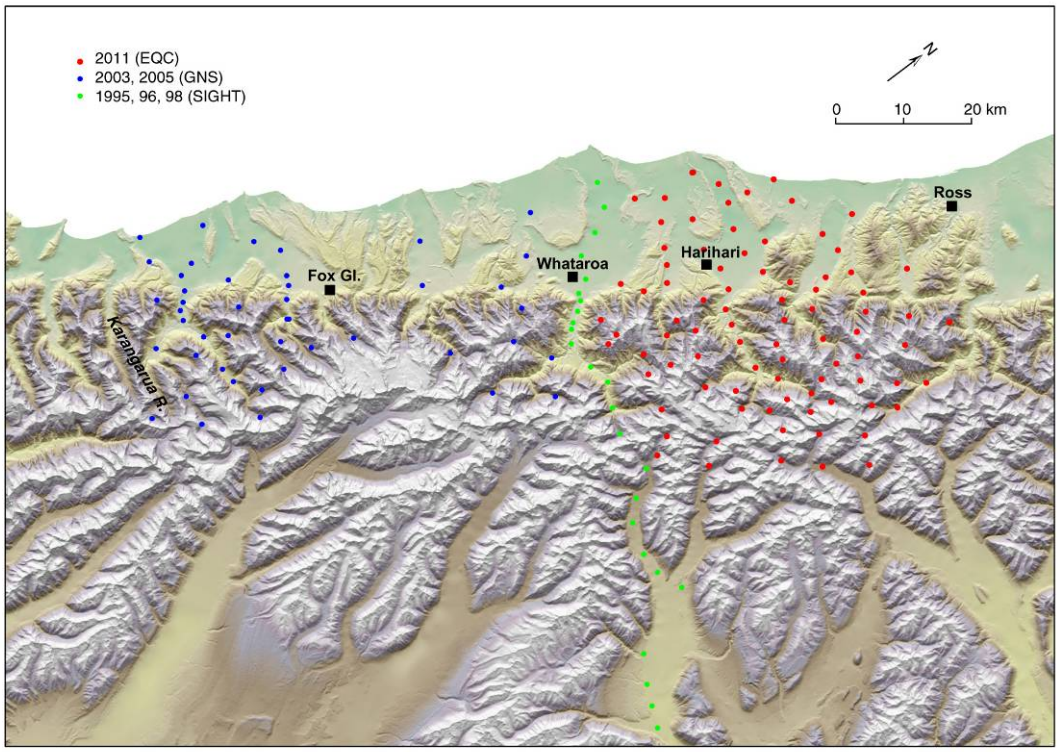

Figure 1: MT measurement locations recorded during March-April 2011 as part of the EQC funded project are shown in red. Earlier measurements undertaken by GNS in 2003 and 2004 are shown in blue and measurements recorded during the SIGHT project are shown in green. The Alpine fault can be seen as the sharp break in the topography running across the page.

The Alpine Fault on the West Coast of New Zealand's South Island (Figure 1) is a mature ~800 km long strike-slip fault which is thought to rupture every ~300 years in earthquakes with estimated magnitudes (M_w) > 7; the last rupture is thought to have taken place ~300 years ago in an earthquake with an estimated magnitude (M_W) ~7.9 [*e.g. Sutherland et al.*, 2007*; Berryman et al.*, 2012].

The central portion of the fault is oriented (N55ºE) 10-15º counter-clockwise from the present-day AUS-PAC plate motion direction [*Beavan et al.*, 2002; *Cande and Stock*, 2004; *DeMets et al.*, 1994]. The deformation is therefore transpressive, with components of interplate motion of 35-39 mm/yr and 6-10 mm/yr parallel and perpendicular to the Alpine Fault respectively [*Beavan et al.*, 2002; *Cande and Stock*, 2004; *DeMets et al.*, 1994; *Walcott*, 1998]. Paleoseismic data indicate late Quaternary strike-slip and dip-slip rates of respectively 27±5 mm/yr and 6-12 mm/yr on the central part Alpine Fault accounting for 70-75 % of the fault-parallel inter-plate motion [*Norris and Cooper*, 2001]. The remainder of the interplate motion is accommodated by high shear strain southeast of the Alpine Fault [*Beavan et al.*, 2007] and also by thickening of the crust into a crustal root and the Southern Alps.

The oblique slip on the Alpine Fault has resulted in the exhumation of highly deformed rocks (mylonites) from below the brittle to ductile (plastic) transition. Thus rocks from the ductile shear

zone or the root of the Alpine Fault beneath the seismogenic portion of the upper crust are being exhumed [*Norris and Cooper*, 2007]. This provides a rare opportunity to compare the results of geophysical investigations of a large active fault with material that has passed through the region of the crust where large earthquakes nucleate. Prior to this work, the depth at which the seismic-aseismic transition near the Alpine Fault has been uncertain due to the wide spacing of seismometers in NZ's national network (GeoNet), and the low levels of seismicity near the Alpine Fault.

Maximum uplift rates in the range 4-10 mm/yr [*Beavan et al.*, 2007; *Wellman*, 1979] are found east of the Alpine Fault and 50-100 km to the south of this study. Present erosion rates are thought to match the uplift rates, such that topography is maintained in a near steady-state [*Koons*, 1989, 1995]. Tectonic uplift and associated exhumation between the Alpine Fault and the Main Divide have raised isotherms and weakened the crust in this region [*Koons*, 1987].

Rocks exhumed southeast of the Alpine Fault show decreasing metamorphic grades with increasing distance from the Alpine Fault with amphibolite grade rocks adjacent to the Alpine Fault mylonite zone (~1 km thick) and greenschist facies ~10 km southeast of the fault. Lower grade prehnite-pumpellyite facies rocks occur further to the southeast [*Cox and Sutherland*, 2007].

Dislocation modelling of geodetic data suggests a locking depth of 5-8 km for the Alpine Fault [*Beavan et al.*, 1999] which suggests that the transition from frictional (brittle) to plastic (ductile) behaviour occurs at ~5-8 km depth. High heat flow [*Townend*, 1999] and the presence of hot springs also suggest a shallow brittle-ductile transition in the central part of the Alpine Fault. This is corroborated by fluid inclusion analyses of exhumed samples that point to temperatures of about 300-350 ºC at 5-8 km depth [*Craw*, 1997; *Jenkin et al.*, 1994; *Toy et al.*, 2010].

Thermal modelling of the Southern Alps [*Koons*, 1987; *Shi et al.*, 1996] also suggest a shallow brittle-ductile transition with temperatures of 350-400 ºC at 5-6 km depth 15 km southeast of the Alpine Fault [*Koons*, 1987]. However these models do not include the effect of heat transport by fluid movement within the upper crust and in our opinion should be viewed as providing an upper bound on the depth of the transition. One of the main aims of this project was to better determine the depth at which the transition from brittle to ductile behaviour occurs.

In actively deforming regions, shear strain in the ductile region of the crust (below the seismogenic zone) will promote the electrical interconnection of any fluid present. Thus, actively deforming ductile-shear-zones that contain even small amounts of fluid should be significantly more electrically conductive than their surroundings. Magnetotelluric (MT) measurements across the Alpine Fault during the SIGHT project [*Wannamaker et al*., 2002; *Jiracek et al*., 2007] and Marlborough Fault System [*Wannamaker et al*., 2009] show that zones of high conductivity occur within the ductile region of the crust at the down-dip projection of these faults. Thus, the SIGHT and Marlborough MT data appear to be imaging zones of high strain rate (ductile shear zones) beneath the seismogenic part of these strike-slip faults and provide evidence for the existence of fluid at lithostatic pressures in the root zones of the faults. Thus the MT data provide information that can be used to constrain interpretations of the geodetic data and future mechanical modelling of the Alpine Fault and complement the information that can be obtained seismologically.

MT data acquisition and analysis

As part of this EQC funded project, MT data were collected from 85 new measurement sites on both sides of the Alpine Fault between Whataroa and Ross; extending ~30 km south east of the Alpine Fault (red dots in Figure 1). The new MT measurements add to MT data collected during the SIGHT project [*Wannamaker et al*. 2002, *Jiracek et al*. 2007] and data collected by GNS in 2003 and 2005

between the Karangarua River and Whataroa; an along-strike MT data coverage of ~120 km (Figure 1).

The EQC funded MT survey took place in March and early April 2011 using GPS-synchronized Phoenix Geophysics MT data-acquisition systems from GNS and the Tokyo Institute of Technology. Measurement sites in mountainous areas were deployed by helicopter. Helicopter deployments were based at Harihari for sites west of the main divide and at Glen Ariffe Station in the upper Rakaia Valley for the 8 sites east of the divide. The remaining sites on the coastal plain were accessed by vehicle. Remarkably, only 2 days were lost to bad weather during this one month campaign and all but one of the planned measurement sites were occupied.

Remote-reference techniques [*Gamble et al*., 1979] as implemented by Phoenix geophysics were used for MT data processing. As a precaution to mitigate the possible effect of current fluctuations in the high power DC transmission line (located about 60 km east of the survey area), remote-reference data were collected at an electrically quiet location in central North Island, ~700 km away from the survey area. Current fluctuations in the DC transmission line, which runs roughly parallel to the Alpine Fault, are a coherent source of polarized electromagnetic waves (EM) that violate the plane-wave condition needed for MT analysis. Fortunately, the EM waves produced by the DC transmission line are highly polarized with a magnetic field polarization perpendicular to the orientation of the line, which runs roughly parallel to the Alpine Fault. For this reason *Wannamaker et al*. [2002] used the orthogonal polarization in their analysis of the SIGHT MT data. Subsequent GNS MT surveys in the South Island in 2003, 2005 and during the Marlborough survey [*Wannamaker et al*., 2009] use GPS synchronized MT data recorders which allowed the remote reference site to be location in the central North Island. Subsequent GNS surveys have shown that removes the effect of the DC transmission line, something that was not possible with the MT equipment used for the SIGHT survey.

In Figures 2-6 we show maps of MT phase tensor ellipses [*Caldwell et al*., 2004] at increasing periods. These ellipses show the variation of the phase response as the direction of magnetic field polarization changes which depend upon the conductivity structure within the earth. The maps at each period show the phase response at a depth range that depends on the value of the overlying resistivity and the period. An approximate estimate of the depth range at each period is given by the skin-depth $\delta \approx 0.5\sqrt{(\rho T)}$ in km, where ρ is an estimate of the overlying (average) resistivity and T is the period. *Caldwell et al*. [2004] show that the tensor phase is unaffected by the localised distorting effect of near surface conductivity heterogeneities or topography for periods where the skin depth is larger than the length scale of the feature producing the distortion. Thus the phase tensor maps shown in Figures 2-6 provide a way of directly visualizing the main features of the conductivity structure at different depth levels (or slices) prior to detailed non-linear inversion of the data.

The effect of the DC transmission line in the SIGHT data phase tensors (outlined in white in Figures 2-6) can be seen in the discrepancy between the SIGHT and 2011 data minimum phase values that is most obvious in Figure 4, the period range where the natural MT signal is weakest. Phase values are in better agreement when only the TM polarization phases are compared.

The size of the tensor ellipses shown in the Figures (2-6) have been normalized by the value of the maximum phase (major axis) with the colour filling the ellipses indicating the magnitude of the minimum phase, one of the tensor's principal values. In areas where the conductivity is increasing with depth, phase values are high (> 45°). High phase values (warm colours) on the coastal plain (seen in Figures 2 and 3) are associated with highly conductive sediments (resistivity 1-10 Ωm) that in-fill the Westland Basin. Southeast of the Alpine Fault, where the bed-rock is exposed, the resistivity is $\sim 10^3$ Ωm [*Wannamaker et al*., 2002; *Jiracek et al*., 2007] and the skin (and thus detection) depth is much greater for the corresponding frequencies.

a)

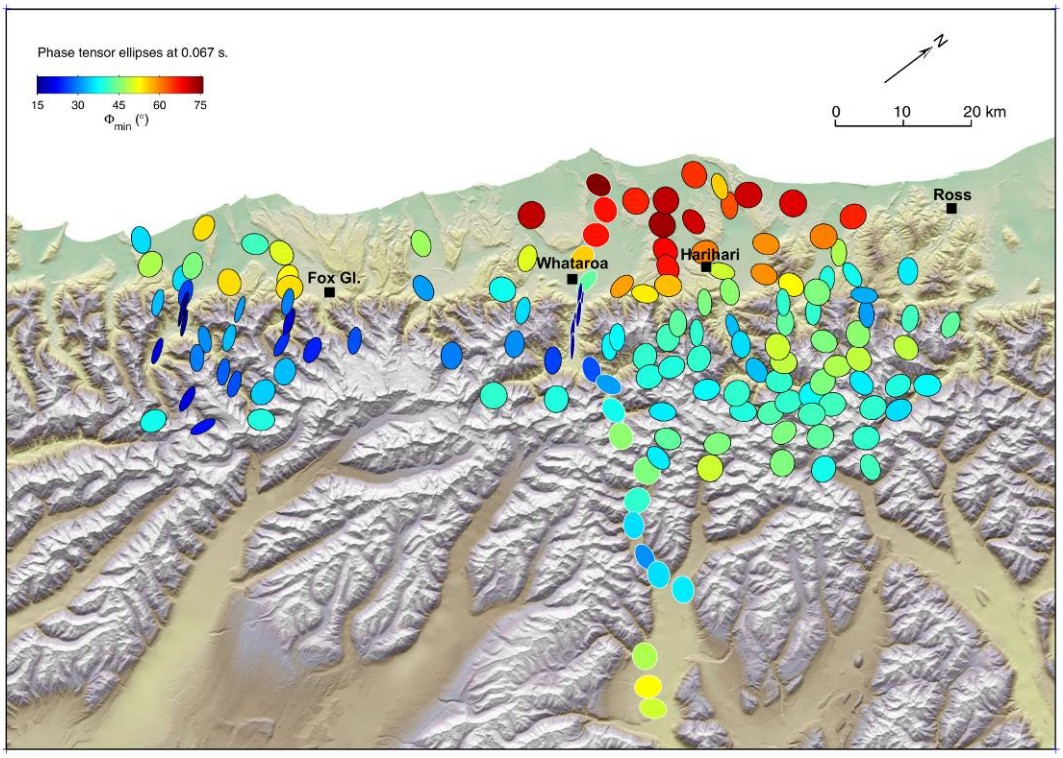

b)

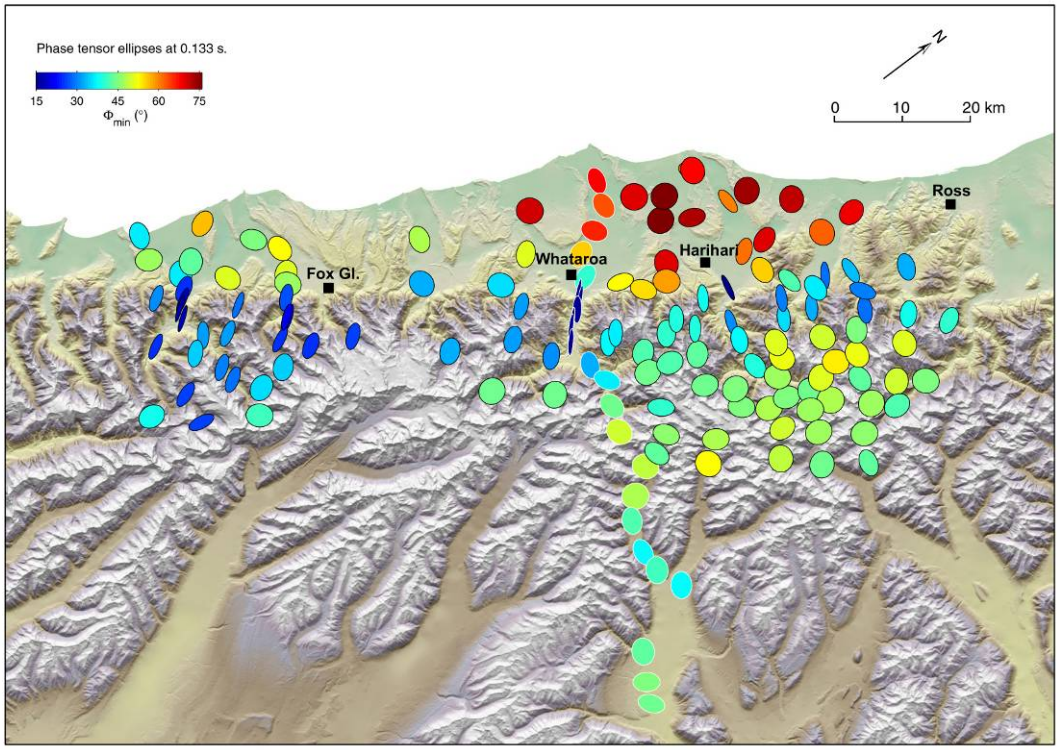

Figure 2: Phase tensor ellipses at (a) 0.067 and (b) 0.133 s periods. SIGHT data are shown outlined in white. The ellipse colour shows the minimum phase (Φ_{min}). Warm colours indicate areas where the electrical conductivity is increasing with increasing depth. The tensor ellipse orientation and ellipticity indicate the direction and magnitude (respectively) of the conductivity change (i.e. horizontal gradient). High phase values (Φ_{min} >50°) on the coastal plain are associated with the highly conductive sediments which in-fill the Westland Basin.

a)

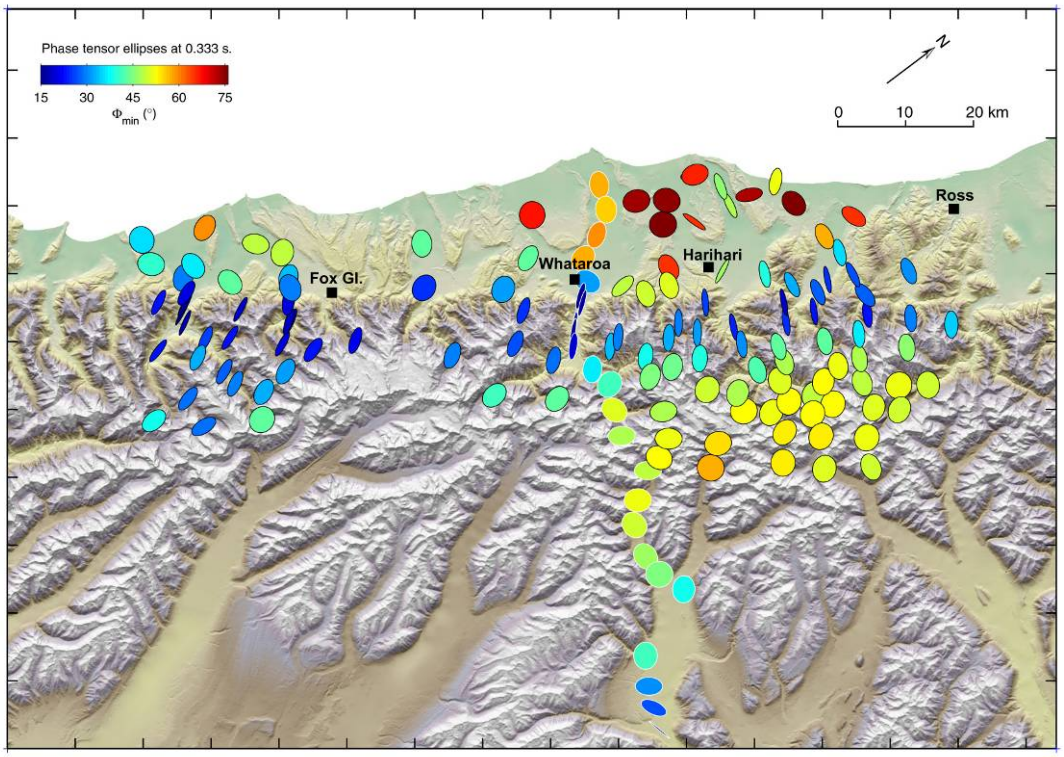

b)

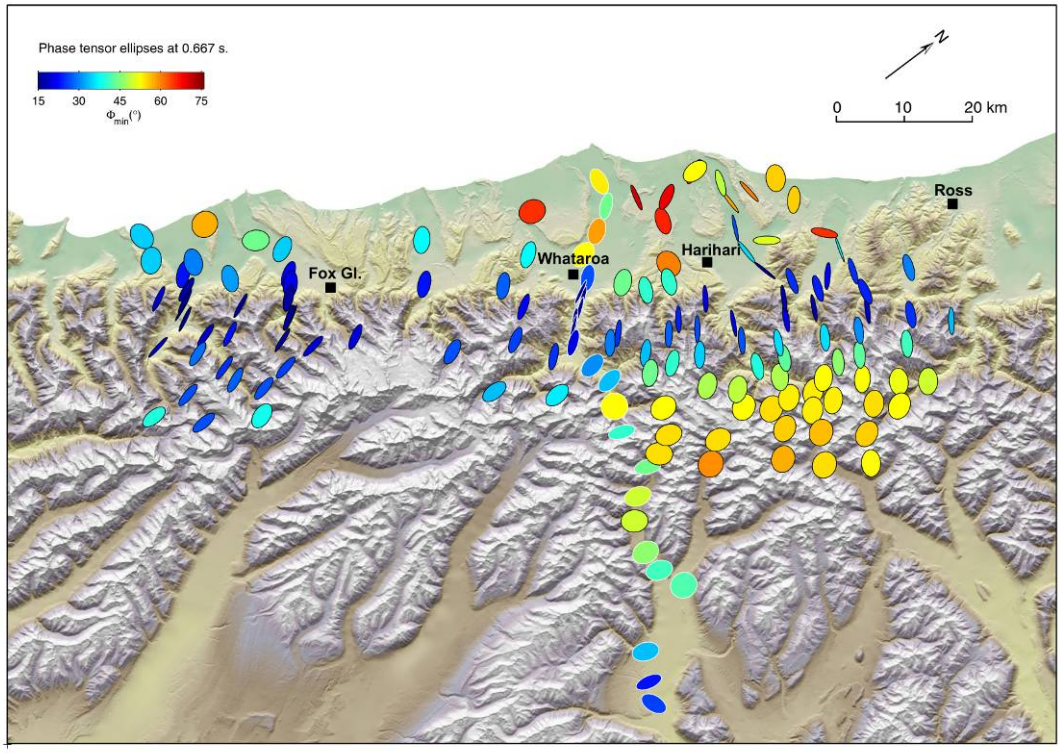

Figure 3: Phase tensor ellipses at (a) 0.333 and (b) 0.067 s periods. The ellipse colour shows the minimum phase (Φ_{min}) with warm colours indicating areas where the electrical conductivity is increasing with increasing depth. Note the development of the area of high phase ~10 km southeast of the Alpine fault in between Whataroa and Ross compared to the shorter period maps (shallower slices) shown in Figure 2. The area of high phase indicates the presence of a conductive zone in the mid-crust.

a)

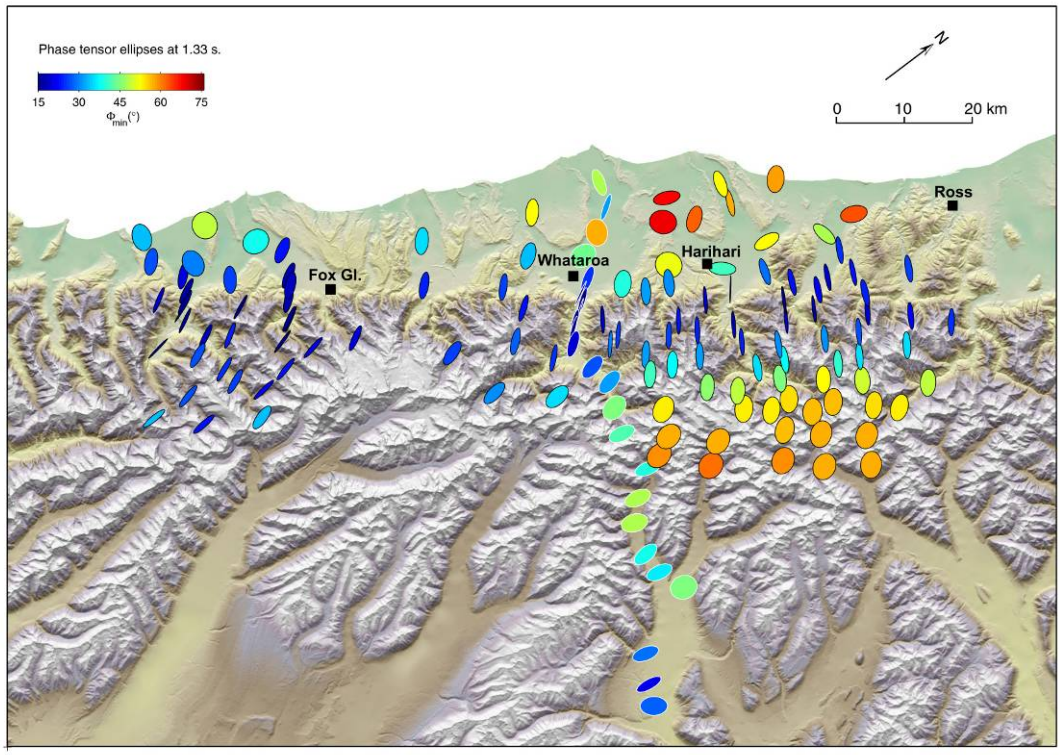

b)

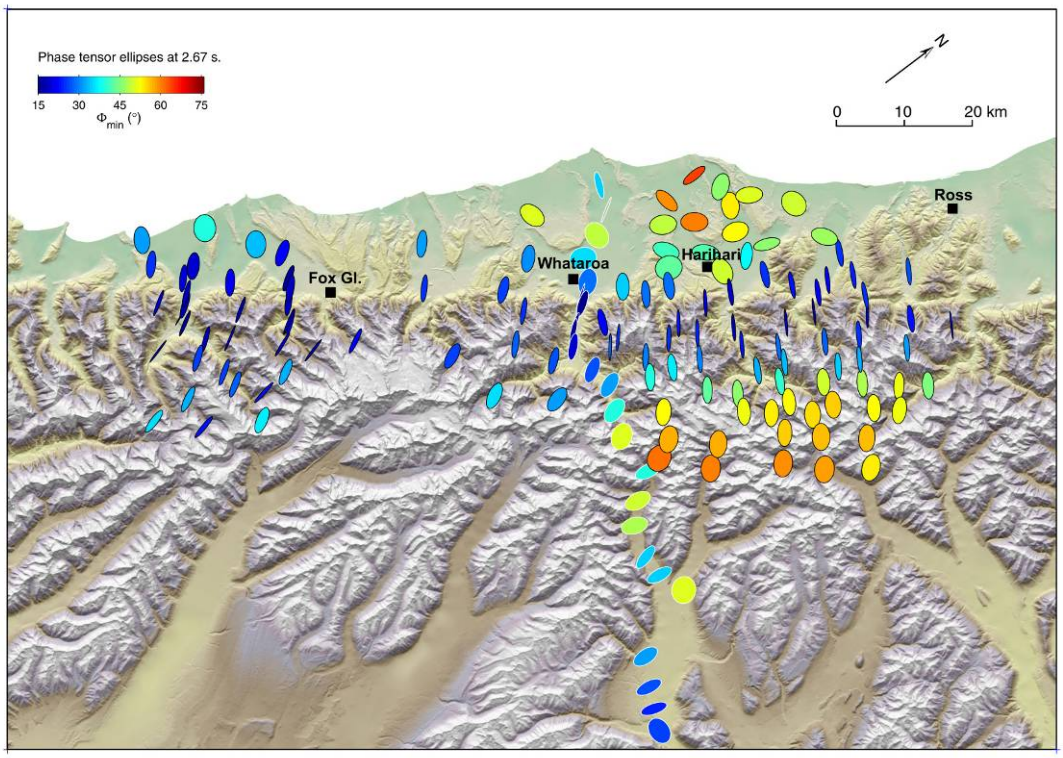

Figure 4: Phase tensor ellipses at (a) 1.33 and (b) 2.67 s periods. The ellipse colour shows the minimum phase (Φ_{min}). Note that the area of highest phase is further to the southeast than in Figure 3 consistent with a south eastward dipping conductive zone similar to that inferred from the SIGHT data (shown outlined in white).

a)

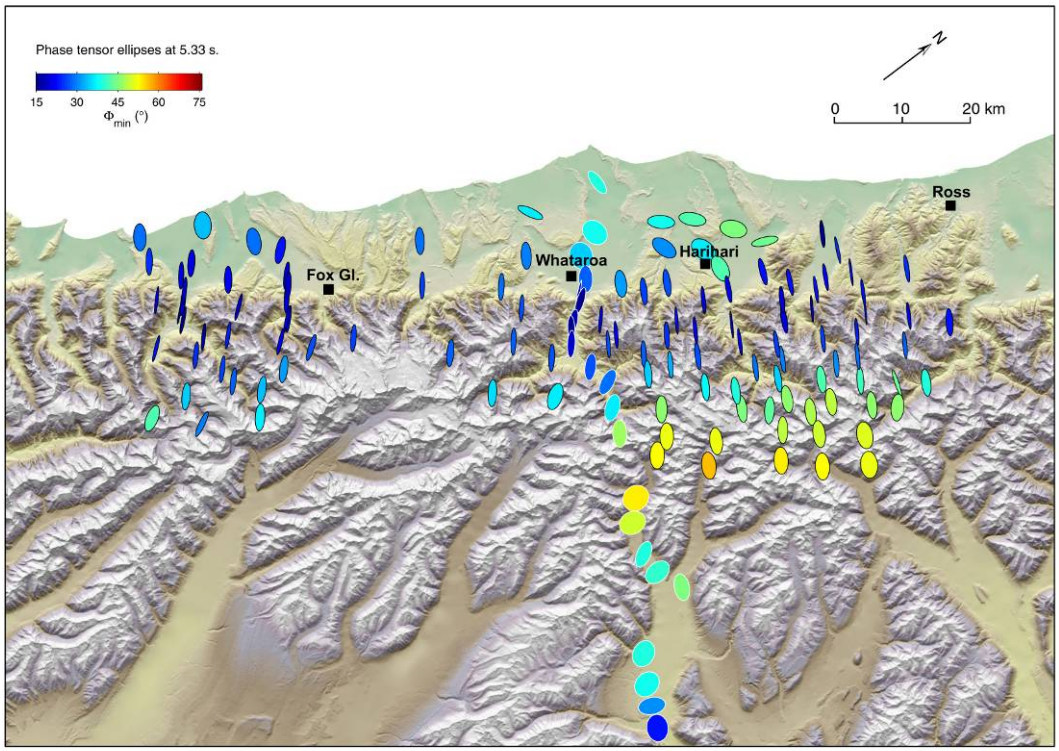

b)

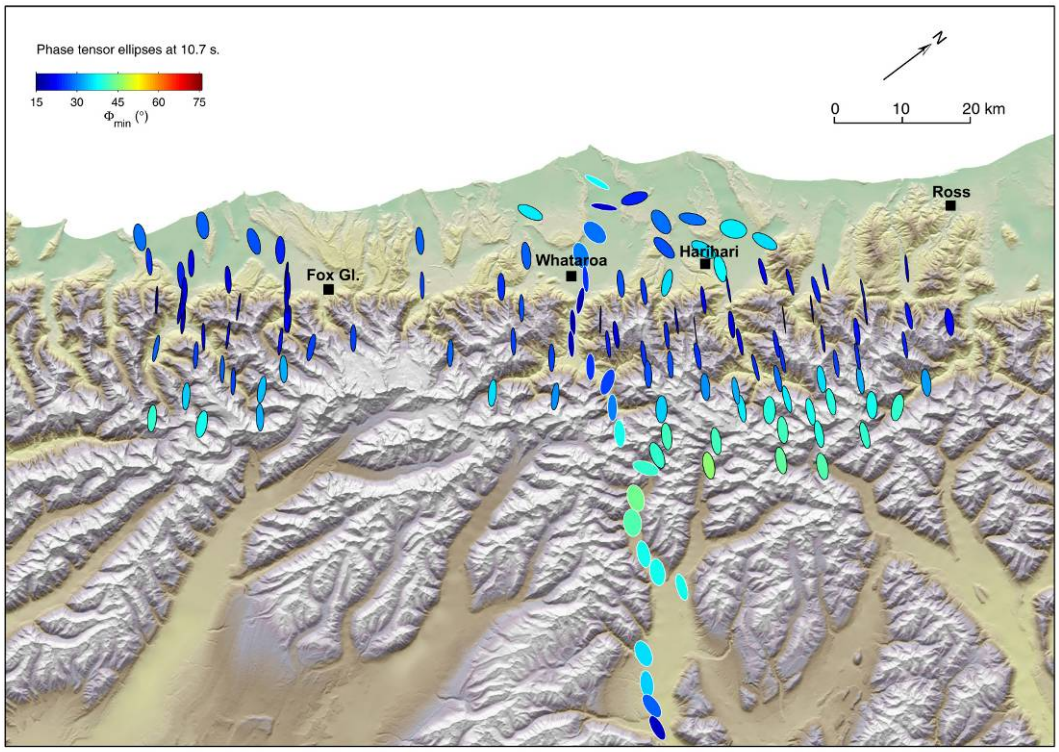

Figure 5: Phase tensor ellipses at (a) 5.33 and (b) 10.7 s periods. The ellipse colour shows the minimum phase (Φ_{min}). Note that the minimum phase values in (b) are less than 45° which indicates that the conductive zone is underlain by more resistive material.

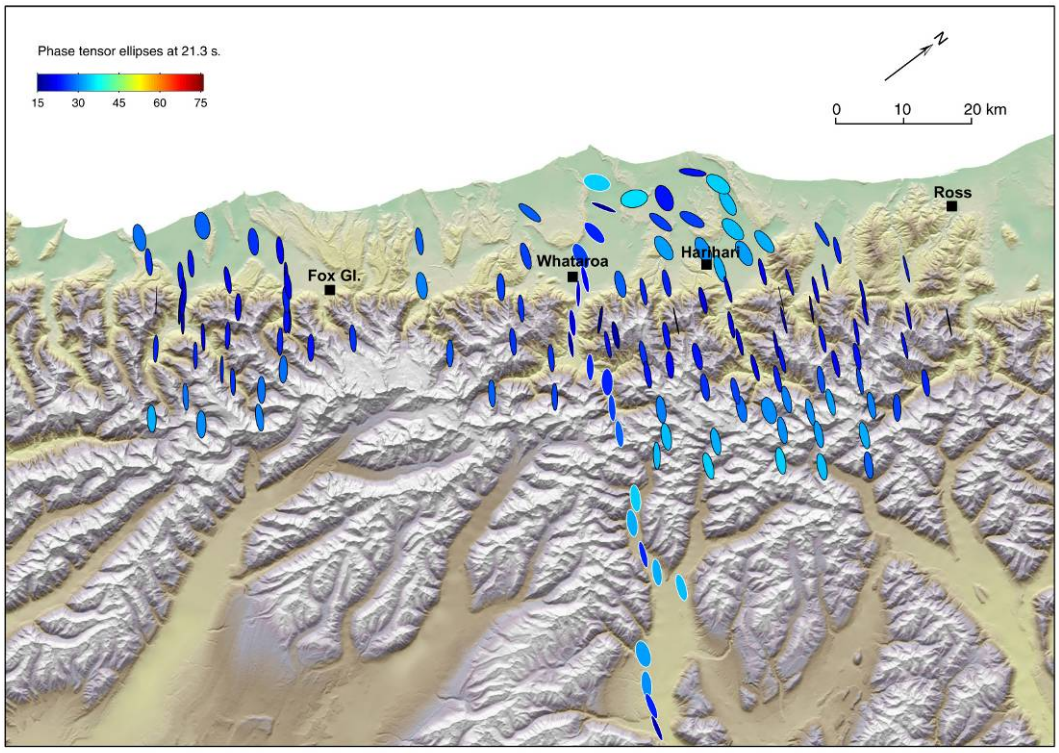

Figure 6: Phase tensor ellipses at 21.3 s period.

As be seen in Figures 3 and 4, an area with high phase (i.e. phase > 45°) develops ~10 km south-east of the Alpine Fault between Whataroa and Ross (Figures 3 and 4) as period increases. At longer periods (Figure 5 and 6) the phase decreases again. This behaviour indicates the presence of a conductive zone southeast of the Alpine Fault at ~8 km depth (assuming a resistivity of 10^3 Ωm) that is underlain by higher resistivity at greater depth. Note that the area of highest phase is further to the southeast than in Figure 3. This south-eastward shift in the phase peak suggests that a south eastward dipping conductive zone similar to that inferred from the SIGHT data by *Wannamaker et al*. [2002] is also present in the region between Whataroa and Ross.

In the period range between Figures 3 and 4, the degree of ellipticity increases markedly between the fault and the area of high phase and the major axes of the ellipses align perpendicular to the fault. The ellipse orientation and ellipticity indicate the direction and magnitude respectively of the horizontal conductivity gradient. The behaviour of the tensor ellipses seen southeast of the Alpine fault in the period range shown in Figures 3 and 4 also indicate that a conductive zone is present further to the southeast and importantly show that the resistivity is high between the surface trace of the fault and the conductive zone further to the southeast similar to the conductivity structure inferred from the SIGHT data [*Wannamaker et al*., 2002; *Jiracek et al*., 2007]. At the longest period shown (Figure 6) the MT data reflect the large scale conductivity structure of the entire region and vary smoothly with location.

In the corresponding area south of Fox Glacier, minimum phase values in the same period range (Figures 3 and 4) are smaller and the orientation of the ellipse axes significantly different from those northeast of Whataroa. This difference in the phase response shows that the conductivity structure southeast of the Alpine Fault is different in the two regions. If a conductive zone is present in the southern region, the behaviour of the phase response suggests that it lies further to the southeast of the MT data coverage (i.e. further inland) than it does in the northern region southeast of the fault between Whataroa-Ross.

Seismic data and analysis

To complement the MT analysis and interpretation, we have examined the seismicity distribution, and seismic properties near the base of the seismogenic zone, focusing on a 60-km long segment of the Alpine Fault between Harihari and Ross. Seismic data from two temporary seismometer arrays: ALFA08 and ALFA09 and from GeoNet stations in the region were used for the analysis reported here. The locations of the ALFA08 and ALFA09 arrays are shown in Figure 7.

The ALFA08 (red triangles in Figure 7) recorded data from October 2008 to October 2009 and consisted of eight broadband and short-period sensors spaced 10-50 km apart. ALFA09 (blue triangles in Figure 7) was a smaller aperture array with a station spacing ~5 km, about 30 x 30 km^2 in area, within the region encompassed by ALFA08. ALFA09 consisted of 10 short-period instruments recording between October 2009 and May 2010. The 5 km station spacing of ALFA09 allows more precise hypocentral location and higher resolution of seismic properties within the array area than ALFA08. However, the data from the more widely spaced ALFA08 array provides better control on seismic properties at deeper levels.

The ALFA'09 array detected about 1380 earthquakes for the October 2009 to May 2010 time period. Initial hypocentre locations of both datasets were determined by manually re-picking P-wave and S-wave arrivals using a 1-D velocity model based on nearby SIGHT Transect 1 (Van Avendonk et al., 2004). Subsequent relocation of the earthquakes was carried out using a 3-D (tomographic) velocity model developed for the region as described below.

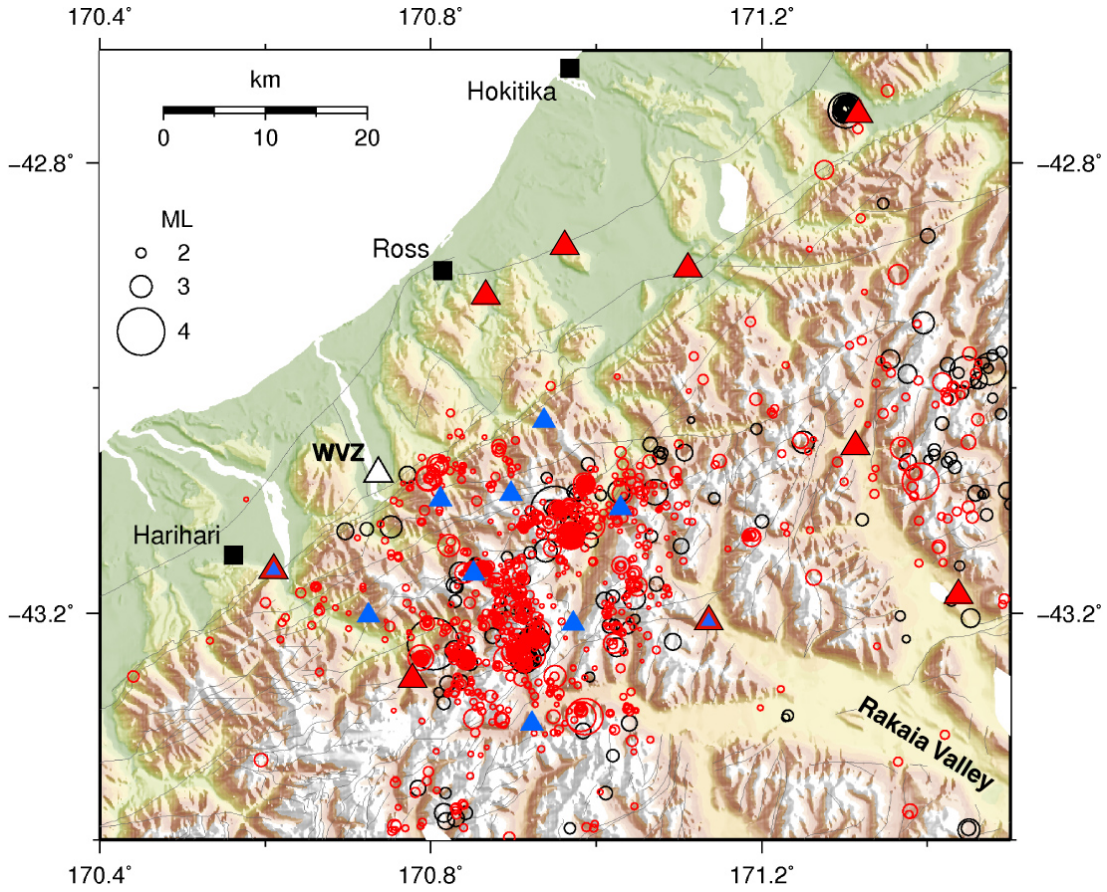

Figure 7: Seismicity located in the study region using data recorded between 2008 and 2010 from the ALFA08 (red triangles) and ALFA09 (blue triangles) arrays. The only GEONET station (WVZ) in the area of figure is shown by the white triangle. The epicentres shown (red and black circles) were determined using the 3D velocity model described in the text. Note the paucity of events in a 10 km wide band immediately southeast of the Alpine Fault compared with the increased event density at distance ranges 10-20 km south-east of the fault.

Seismic Tomography

Hypocentres and seismic properties (P-wave velocity Vp, shear wave velocity Vs, and velocity ratio Vp/Vs) were determined in 3-D using the double-difference tomographic method tomoDDPS [*Zhang and Thurber*, 2003] based on the double-difference location procedure of *Waldhauser and Ellsworth* [2000]. The events used for the seismic tomography consisted of 252 ALFA08 and 541 ALFA09 earthquakes with 15 or more associated picks with epicentres < 20 km distant from any station. In addition, we included data from 158 aftershocks of the 1994 Arthur's Pass earthquake with >= 20 associated phases and residual rms errors less than 0.11 s. Also included were a small group of 19 earthquakes located near the northern most ALFA08 station (Figure 7), with ≥ 14 observations. Finally, we included 102 earthquakes recorded in 1995/1996 by the SAPSE (Southern Alps Passive Seismic Experiment) array (station spacing of 10-60 km, Anderson et al., 1997). The SAPSE earthquakes selected all had ≥ 15 associated phases with hypocentres located less than 25 km from any station. In total, data from 1062 earthquakes were used for the tomographic inversion.

The initial or starting model used for the inversion was the New Zealand wide 3-D model [*Eberhart-Phillips et al*., 2010] which we interpolated onto a 3-D grid with its y-axis oriented parallel (N54ºE) to the Alpine Fault and with variable grid spacing. In regions of high station density grid nodes were spaced 5 km laterally and in 2 km depth increments down to 12 km depth with greater increments below. We included catalogue absolute and differential travel times in the tomographic inversion, and initially limited the maximum offset between linked event pairs to be 25 km. The average offset between pairs was 7 km.

To estimate the optimal combination of damping and smoothing parameters needed for the inversion, a set of one-iteration trial inversions were carried out. On the basis of these trials the damping and smoothing parameters were set at 500 and 20 respectively, within the range expected for these parameters [*Eberhart-Phillips*, 1986; *Thurber et al*., 2009].

Resolution analysis

We tested the resolution of the tomographic modelling on our data using standard checkerboard tests. These tests show that within the area of the ALFA09 array the tomographic analysis recovered ~90 % of the Vp checkerboard amplitude in a 2-10 km depth range. Resolution of Vs and Vp/Vs is not as good with ~80 % and 40-80 % of the Vs and Vp/Vs amplitude recovery between 2 and 6 km depth (respectively).

Outside the area of the ALFA09 array, resolution is less certain particularly to the south of the array where ray coverage is less. Resolution to the north is better because of the number of source events to the north of the array. At depths shallower than 2 km velocities and Vp/Vs are less well determined.

Tomographic results

Results from the tomographic analysis are shown in Figure 8 as a NW-SE (N145E; strike perpendicular) cross-section through the centre of the ALFA09 array and as a series of depth slices in Figure 9.

As can be seen in Figure 8, for depths less than 10 km values of Vp, and Vs are relatively low (less than 5.5 km/s and 3.4 km/s, respectively) in a 10 km wide band immediately south-east of the Alpine Fault. Values for Vp and Vs in this band are characteristic of laboratory values measured for high metamorphic grade (garnet-zone) Alpine Schist rather than Alpine Fault mylonite *[Christensen and Okaya*, 2007], which suggests that the 5 km node spacing used in the inversion is too coarse to resolve

any velocity anomaly associated with the mylonite zone (expected to be ~1 km thick) adjacent to the Alpine Fault plane. Vp/Vs values in the top 8 km in this band are also relatively high (~1.75), although this Vp/Vs value is not in itself highly anomalous.

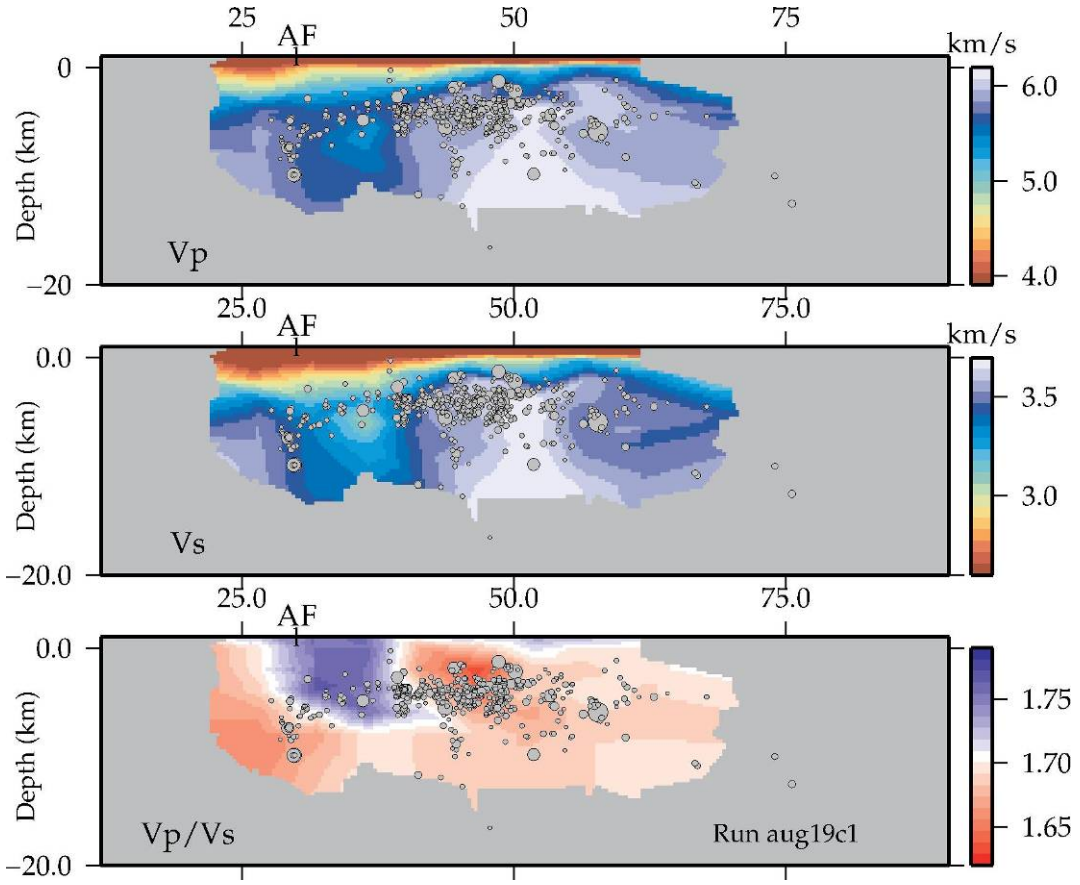

Figure 8: NW-SE cross-sections of Vp (top); Vs (middle), and Vp/Vs (bottom), on a NW-SE (N145E striking) profile, passing through GeoNet station WVZ (Figure 7). Values are masked grey where they are poorly resolved. Projections of earthquake hypocenters onto the vertical cross-section are plotted as grey circles, with symbol size proportional to the log of the magnitude. **AF** is the projection of the surface trace of the Alpine Fault onto the cross-section.

Distribution of seismicity

The 1062 earthquakes used in the velocity inversion were relocated as part of the tomographic inversion and are also shown in Figures 8 and 9. Within the ALFA09 array the completeness-magnitude is 1.5, a unit of magnitude lower than the GeoNet catalogue completeness-magnitude in this region. The new locations provide a more precise picture of the distribution of seismicity, both spatially and with depth, than previously possible.

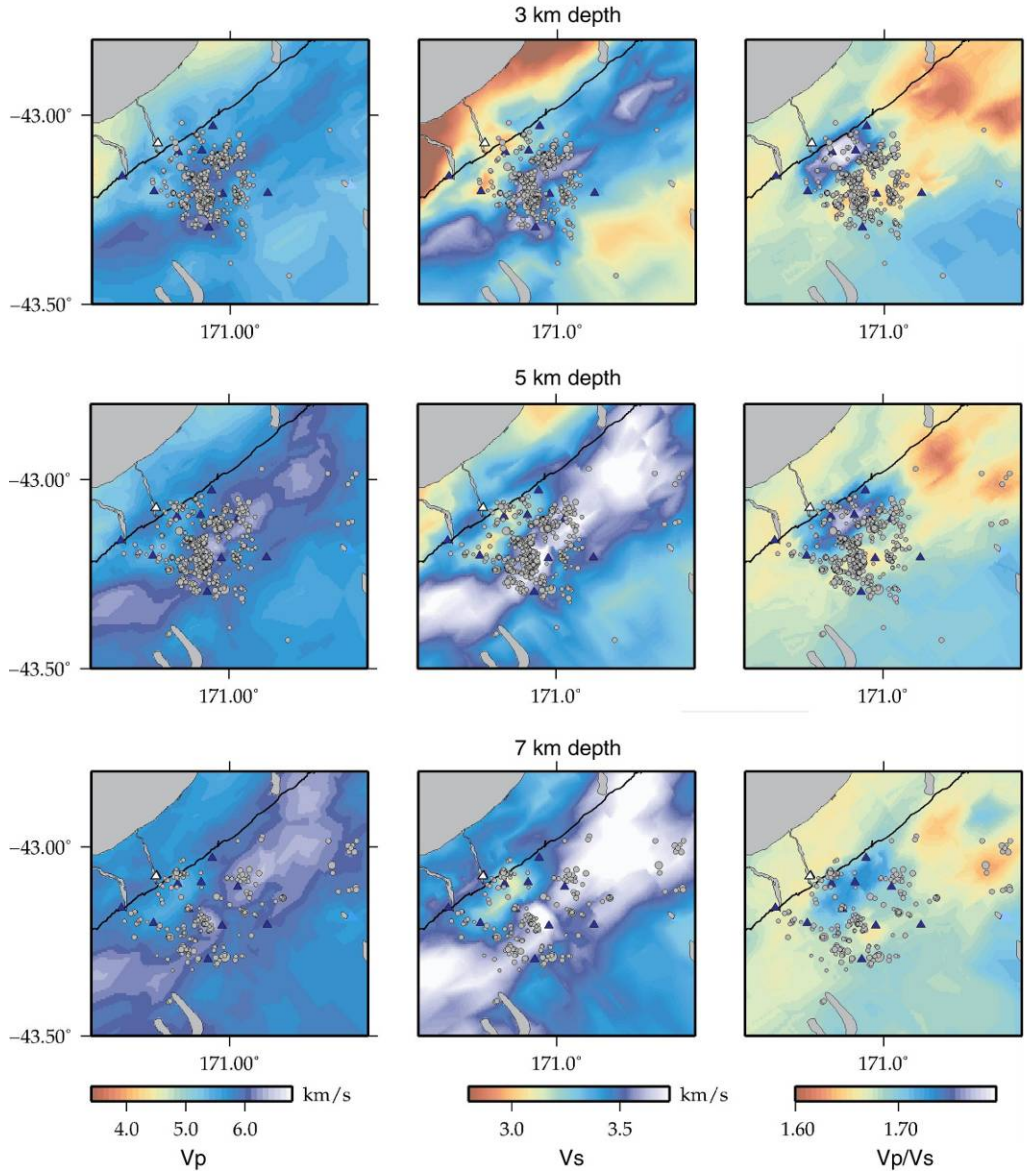

Figure 9: Seismic velocities and Vp/Vs ratio determined from double-difference tomography. Top, middle and bottom rows show 3, 5 and 7 km depth slices, respectively. ALFA09 and WVZ seismometer locations are shown as small triangles. Resolution of Vp, Vs and Vp/Vs in the area shown in the figure changes considerably – good resolution within the ALFA09 array, with lower resolution to the south-west and south-east outside the area delimited by the seismometers. Earthquake locations within 2 km of each depth slice are shown by grey circles.

Only a small number of earthquakes occurred close to the Alpine Fault during the six-month recording period of the ALFA09 array. Within 5 km of the Alpine Fault trace 90% of the events recorded were shallower than 10 km (Figure 10). Previous studies of microseismicity near the Alpine fault [*Boese et al*., 2012; *Eberhart-Phillips*, 1995] also found little or no seismic activity in the region beneath the fault trace and a maximum seismogenic depth of ~10 km, in good agreement with our results.

As can most clearly be seen in Figure 11, a notable feature of the distribution of the relocated seismicity is the relative paucity of earthquakes at depth less than ~4 km in a 10 km wide band immediately southeast of the Alpine fault. Compared with this band, the seismicity to the southeast is more intense with significantly more events located at shallower depth (Figure 10).

Discussion

The paucity of earthquakes within ~10 km of the Alpine Fault trace has been noted previously in other studies [*Adams*, 1980; *Evison*, 1971; *Eberhart-Phillips*, 1995; *Leitner et al*., 2001; *O'Keefe*, 2008; *Boese et al*., 2012]. These studies also suggest that the band of low-seismicity adjacent to the Alpine Fault widens south-eastwards forming a 20 km wide 'low-seismicity triangle' between the Whataroa and Karangarua Rivers [*Eberhart-Phillips*, 1995; *Leitner et al*., 2001; *O'Keefe*, 2008; *Boese et al*., 2012].

The increased width of the low-seismicity region in the south corresponds with a change in rock foliation north and south of Whataroa, with more gently dipping foliations observed to north, and westward dipping bedding, abundant faulting and steeply dipping foliations to the south, where the uplift rate and level of exhumation are greater [*Leitner et al*., 2001; *Little et al*., 2005]. The MT response also differs north and south of the Whataroa.

North of Whataroa, the north-western margin of the zone of more intense and shallower seismicity (Figure 11) correlates with the onset of high MT phase seen best in Figures 3 and 11. This correlation suggests a relationship between the conductive zone in the ductile lower crust inferred from the MT data and the more intense seismicity in the brittle zone above. Whether this reflects the upward escape of fluid from a ductile shear zone into the brittle crust or a stress response to the ductile zone below requires further detailed research and mechanical modelling.

Our tomography results (Figures 8 and 9) suggest the presence of slightly higher Vp/Vs (~1.75) values between 2-8 km depth in the ~10 km wide region of reduced seismicity southeast of the Alpine Fault. Higher Vp/Vs values are often taken as evidence for increased fluid pressure and an associated reduction of frictional strength. However, other explanations for the (slightly) enhanced Vp/Vs values observed are possible perhaps associated with the presence of the high-metamorphic grade schist and a greater density of fractures in this region.

The earthquakes observed in our study area show a marked concentration in a band 10 to 25 km southeast of the Alpine Fault (Figures 7, 8 and 9). Figure 10 shows the depth distribution of the best constrained earthquakes within the area of the ALFA09 array for epicentres within 5 km of the Alpine Fault trace (Figure 10a) and for epicentres 10-25 km southeast of the fault. Ninety five per cent of the earthquakes between 10 and 25 km southeast of the fault occur above 7-8 km depth. Also, as can been seen in the cumulative plots, significantly more earthquakes occur at depths shallower than ~4km in this band (Figure 10b), than in the region close to the Alpine Fault (Figure 10a).

Earthquake frequency and co-seismic stress drop are thought to reach a maximum at the depth of maximum yield strength [*Meissner and Strehlau*, 1982]. In the region between 10 to 25 km southeast of the fault (Figure 10b), the observed seismicity reaches a peak at ~4km depth. Assuming that this depth is controlled by the temperature at which onset of creep occurs in quartz, this suggests the temperature at 4 km depth is ~250-300 °C. Similarly, assuming that the 95% depth limit of seismicity marks the base of the seismogenic zone and the onset creep in feldspar, temperatures at ~7-8 km depth would be ~450-500 °C. This estimate of the depth for the ductile transition agrees well with the maximum seismogenic depths observed in previous micro-seismic studies of the Southern Alps [*Leitner et al*., 2001 and *Boese et al*., 2012] and is comparable with estimates of the brittle-ductile transition depth (between 5 and 8 km) based on fluid inclusion temperatures [*Craw*, 1997; *Jenkin et al*., 1994; *Toy et al*, 2010] and thermal modelling [*Koons*, 1987].

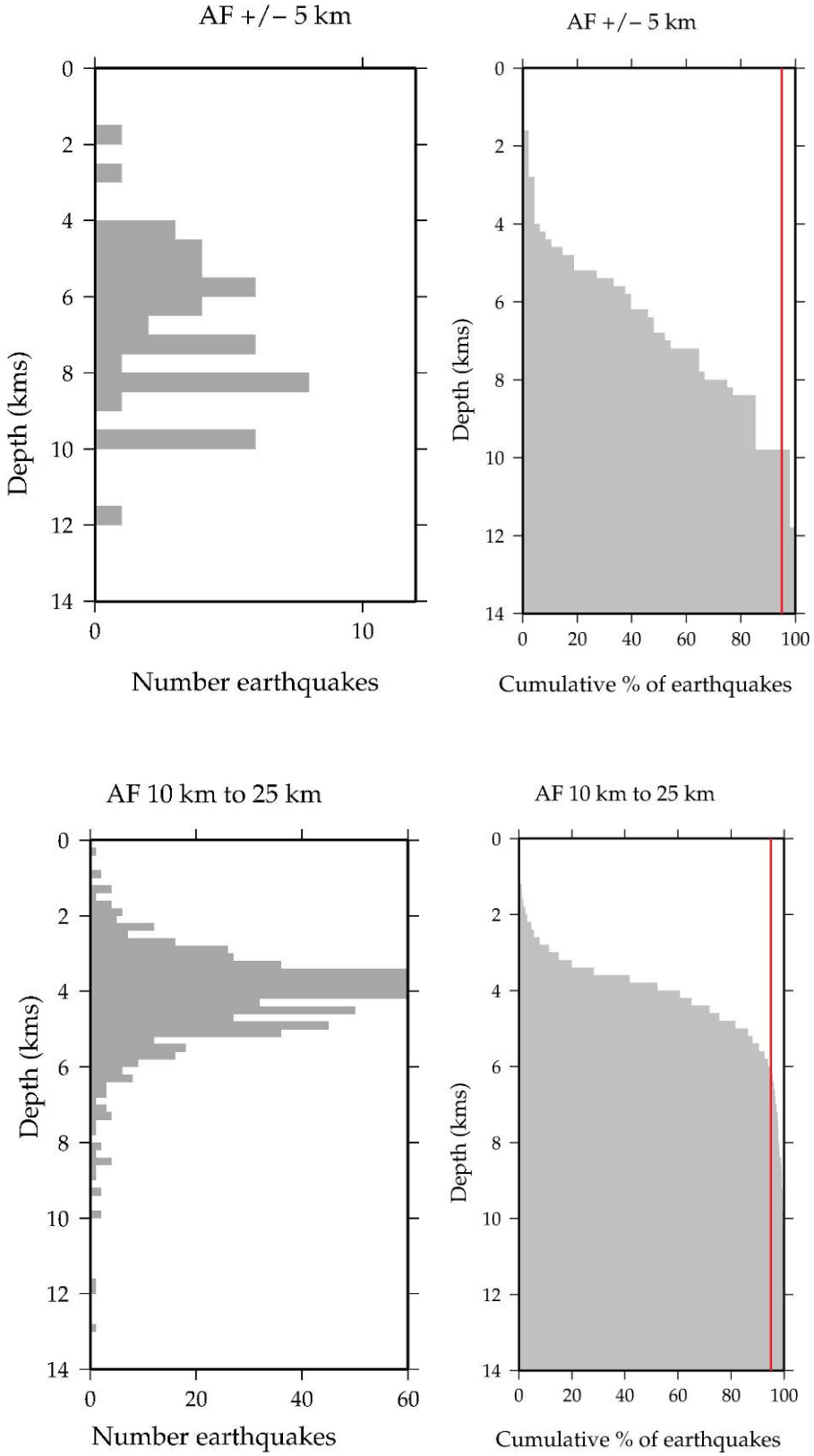

Figure 10: Depth distribution for relocated earthquakes, in the distance ranges: (a) -5 to 5 km (b) 10-25 km, from the Alpine Fault, along the Harihari-Ross segment of the Alpine Fault.

The paucity of earthquakes close to the Alpine Fault does not allow the depth of the maximum seismicity to be determined with confidence (Figure 10a). However, as can be seen in Figure 11, the 95% depth limit of seismicity does not appear to change significantly with distance southeast of the fault.

We note that ~45 km north of the ALFA09 array, in the aftershock region of the 1994 Arthur's Pass earthquake [*Bannister et al*, 2006], at a similar distance inland from the Alpine Fault, 97 % of hypocentres are located at depths less than 10 km suggesting that the transition to ductile behaviour in the Arthurs Pass region, north of the present study, is ~2 km deeper than beneath the ALFA09 array.

Conclusions

The key observational results from the work supported by EQC are summarized in Figure 11. The distribution of seismicity of the relocated events shows that more than 70% of the events are concentrated in a tight band of seismicity between 10 and 25 km southeast of the Alpine Fault. Below ~4 km depth the seismicity is present as far northwest as the Alpine Fault. Assuming the Alpine Fault dips to the southeast at about 45° [e.g. *Norris and Cooper*, 2001] this means that some seismicity is located within the footwall of the fault. Seismicity peaks at ~4km depth (Figure 10) suggesting the onset of creep in quartz occurs at about this depth and, if so, temperatures at ~ 4 km are 250-300 °C. Ninety five per cent of all the seismicity occurs above 7-8 km depth suggesting the transition to ductile behaviour also occurs at about this depth. If we assume that the onset of ductile behaviour at low strain rates corresponds with the temperature at which creep occurs in feldspars (~450-500 °C) then we can use the base of the seismicity as an indicator of temperature. We emphasise however, that other factors occur such as the presence of over pressured fluid and strain rate will also play an important role in the depth limit of seismicity.

The north western edge of the band of shallow (< 4km depth) seismicity coincides with the edge of a south eastward dipping electrically conductive zone in the mid-crust, similar to the conductive zone inferred from the SIGHT data [*Wannamaker et al*., 2002; *Jiracek et al*., 2007] and at a similar distance southeast of the fault. Simple skin-depth estimates of the depth to the conductive zone suggest that conductivities increase at or near the bottom of the seismogenic zone at about 8 km. Between the conductor and the surface trace of the Alpine Fault the resistivity is high. Thus the new MT data suggest that the main features of the conductivity structure southeast of the Alpine Fault first inferred by *Wannamaker et al*. [2002] extends northward from Whataroa to at least Ross. Following Wannamaker et al. we interpret the conductive zone in the mid-crust as a ductile shear zone containing electrically interconnected fluid.

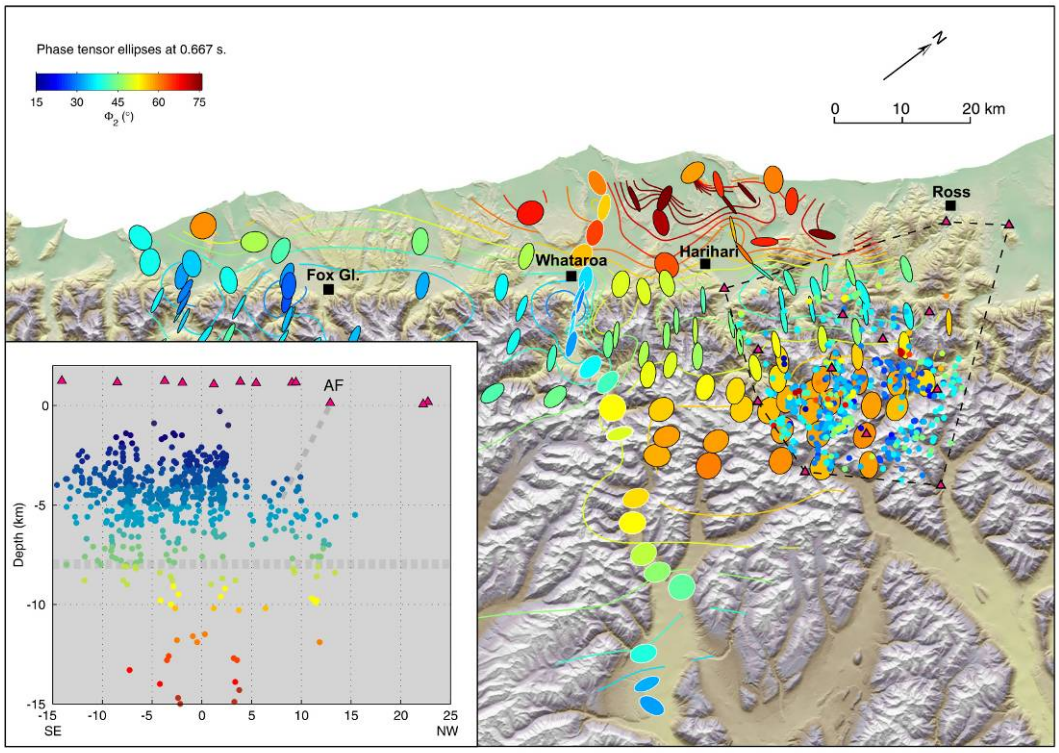

Figure 11: Summary of key results from the EQC MT survey and seismological data analysis. MT phase tensor ellipse colours show the geometric mean (Φ_2) of the maximum and minimum phases at 0.667 s period. Warm colours indicate areas where the electrical conductivity is increasing with increasing depth. High phase values (Φ_2 >60°) on the coastal plain are associated with the highly conductive sediments in the Westland Basin. The area of high phase (Φ_2 >55°) south-east of the Alpine Fault indicates the presence of a conductive zone in the mid-crust. The insert shows the seismicity (coloured dots) with magnitude (Mw) >1 projected on to a profile perpendicular to the Alpine fault located within the area outlined by the dashed black line. The grey horizontal line (dashed) shows the 95% depth limit of seismicity. The position of the Alpine Fault (AF) is indicated by the sloping dashed line; assuming a 45° south eastward dip.

The next step in our work is to complete a 3-D inversion of the 2011 MT data between Whataroa-Ross to define details of the geometry of the conductivity structure. Initial 3-D inversion modelling of the GNS MT data to the south of the Whataroa valley did not converge because of the lack of data in the ice covered area south of Whataroa and in the area southeast of the main divide. More MT measurements southeast of the main divide and in the area between Fox Glacier and Whataroa will be required before the conductivity structure in this region can be resolved. However, it is clear from the data already available that there is a significant difference between the conductivity structure between the northern and southern parts of the MT data coverage.

Within the best resolved part of the seismic array, the maximum depth of seismicity does not appear to change significantly out to a distance of ~25 km southeast of the Alpine fault. This suggests that the thermal structure in the upper crust southeast of Alpine Fault does not vary significantly within ~25 km of the fault, contrary to that predicted by some mechanical models [e.g. *Shi and Allis*, 1996] which assume that heat is transported conductively. Our observations support a model of heat transport within the brittle part of the crust dominated by fluid movement in fractures and cracks rather than thermal conduction through the rock matrix. The presence of hot springs in the region support this view and shows that the fracture system must be connected to the surface and, as a consequence, suggest that the fluid pressure in the brittle region of the crust will be near hydrostatic down to depths of at least 4 km and possibly down to the base of the seismogenic zone at ~ 7-8 km.

References

Adams, J. (1980), Paleo seismicity of the Alpine fault seismic gap, New Zealand, *Geology,* 8(2), 72-76.

Anderson, H., D. Eberhart-Philips, T. McEvily, F. Wu, and R. Uhrhammer (1997). Southern Alps Passive Seismic Experiment, *Science Report 97/21*, Inst. Of Geol. and Nucl.Sci., Lower Hutt, New Zealand, 1997.

Bannister, S.; C. Thurber, and J. Louie, (2006). Detailed fault structure highlighted by finely relocated aftershocks, Arthur's Pass, New Zealand. *Geophys. Res. Lett.,* 33, L18315, doi:10.1029/2006GL027462.

Beavan, J., S. Ellis, and L. Wallace (2007), Kinematic Constraints From GPS on Oblique Convergence of the Pacific and Australian Plates, Central South Island, New Zealand, in *A Continental Plate Boundary: Tectonics at South Island, New Zealand*, edited by D. Okaya, T. Stern and F. Davey, pp. 75-94, AGU, Washington D.C.

Beavan, J., P. Tregoning, M. Bevis, T. Kato, and C. Meertens (2002), Motion and rigidity of the Pacific Plate and implications for plate boundary deformation, *Journal of Geophysical Research B: Solid Earth*, *107*(10), ETG 19-11 - 19-15.

Beavan, J., et al. (1999), Crustal deformation during 1994-1998 due to oblique continental collision in the central Southern Alps, New Zealand, and implications for seismic potential of the Alpine fault, *Journal of Geophysical Research B: Solid Earth*, *104*(B11), 25233-25255.

Berryman K.R., U.A. Cochran, K.J. Clark, G.P. Biasi, R.M. Langridge, P. Villamor (2012), Major Earthquakes Occur Regularly on an Isolated Plate Boundary Fault, *Science, 366,* 1690-1693. [DOI:10.1126/science.1218959]

Boese, C. M., J., Townend, E. Smith, and T. Stern (2012), Microseismicity and stress in the vicinity of the Alpine Fault, central Southern Alps, New Zealand, *J. Geophys. Res.*, *117*(B2), B02302.

Caldwell, T. G., H.M. Bibby, and C. Brown (2004), The magnetotelluric phase tensor. *Geophys. J. Int.* 158 457-469.

Cande, S. C., and J. M. Stock (2004), Pacific-Antarctic-Australia motion and the formation of the Macquarie Plate, *Geophysical Journal International*, *157*(1), 399-414.

Christensen, N. I., and D. Okaya (2007), Compressional and Shear Wave Velocities in South Island, New Zealand Rocks and Their Application to the Interpretation of Seismological Models of the New Zealand Crust, in *A Continental Plate Boundary: Tectonics at South Island, New Zealand*, edited by D. Okaya, T. Stern and F. Davey, pp. 123-155, AGU, Washington D.C.

Cox, S. C., and R. Sutherland (2007), Regional Geological framework of South Island, New Zealand, and its Significance for Understanding the Active Plate Boundary., in *A Continental Plate Boundary: Tectonics at South Island, New Zealand*, edited by D. Okaya, T. Stern and F. Davey, p. 369, AGU, Washington, D.C.

Craw, D. (1997), Fluid inclusion evidence for geothermal structure beneath the Southern Alps, New Zealand, *New Zealand Journal of Geology and Geophysics*, *40*(1), 43-52.

DeMets, C., R. G. Gordon, D. F. Argus, and S. Stein (1994), Effect of recent revisions to the geomagnetic reversal time scale on estimates of current plate motions, *Geophysical Research Letters*, *21*(20), 2191-2194.

Eberhart-Phillips, D.; Bannister, S.C. (2002), Three-dimensional crustal structure in the Southern Alps region of New Zealand from inversion of local earthquake and active source data. *Journal of geophysical research. Solid earth, 107(B10):* doi:10.1029/2001JB000567

Eberhart-Phillips, D. (1986), Three-dimensional velocity structure in northern California Coast Ranges from inversion of local earthquake arrival times, *Bulletin of the Seismological Society of America*, 76(4), 1025-1052.

Eberhart-Phillips, D. (1995), Examination of seismicity in the central Alpine Fault region, South Island, New Zealand, *New Zealand Journal of Geology & Geophysics*, *38*(4), 571-578.

Eberhart-Phillips, D., M. Reyners, S. Bannister, M. Chadwick, and S. Ellis (2010), Establishing a versatile 3-D seismic velocity model for New Zealand, *Seismological Research Letters*, 81(6), 992-1000.

Gamble, T., Goubau, W., and Clarke, J. (1979), Magnetotellurics with a remote reference. *Geophys.* 44, 53-68.

Evison, F. F. (1971), Seismicity of the Alpine Fault, New Zealand, *Bulletin - Royal Society of New Zealand*, 9, 161-165.

Jenkin, G. R. T., D. Craw, and A.E. Fallick (1994), Stable isotopic and fluid inclusion evidence for meteoric fluid penetration into an active mountain belt; Alpine Schist, New Zealand, *Journal of Metamorphic Geology*, *12*(4), 429-444.

Jiracek, G.R.; Gonzalez, V.M.; Caldwell, T.G.; Wannamaker, P.E.; Kilb, D. (2007), Seismogenic, electrically conductive, and fluid zones at continental plate boundaries in New Zealand, Himalaya, and California, USA. p. 347-369 In: Okaya, D.A.; Stern, T.A.; Davey, F.J. (eds) *A continental plate boundary: tectonics at South Island, New Zealand.* Washington, DC: American Geophysical Union. Geophysical monograph 175.

Koons, P. O. (1987), Some thermal and mechanical consequences of rapid uplift: an example from the Southern Alps, New Zealand, *Earth and Planetary Science Letters*, *86*(2-4), 307-319.

Koons, P. O. (1989), The topographic evolution of collisional mountain belts: a numerical look at the Southern Alps, New Zealand, American Journal of Science, 289(9), 1041-1069.

Koons, P. O. (1995), Modeling the topographic evolution of collisional belts, Annual Review of Earth & Planetary Sciences, 23, 375-408.

Leitner, B., D. Eberhart-Phillips, H. Anderson, and J. L. Nabelek (2001), A focused look at the Alpine fault, New Zealand: Seismicity, focal mechanisms, and stress observations, *Journal of Geophysical Research B: Solid Earth*, *106*(B2), 2193-2220.

Little, T.A., Cox, S., Vry, V.K., and Batt, G.E. (2005). Variations in exhumation level and uplift rate related to oblique-slip ramp geometry, Alpine Fault, central Southern Alps, New Zealand, *Geol. Soc. Am. Bull.* 117(4), 707-723.

Meissner, R., and J. Strehlau, 1982. Limits of stress in continental crusts, and their relation to the depth-frequency distribution of shallow earthquakes. *Tectonics*, 1(1), 73-89.

Norris, R.J. and Cooper A.F. (2007). The Alpine Fault, New Zealand: Surface Geology and field relationships. In: Okaya, D.A.; Stern, T.A.; Davey, F.J. (eds) *A continental plate boundary : tectonics at South Island, New Zealand.* Washington, DC: American Geophysical Union. Geophysical monograph 175, 157-175.

Norris, R. J., and A. F. Cooper (2001), Late Quaternary slip rates and slip partitioning on the Alpine Fault, New Zealand, *Journal of Structural Geology*, *23*(2-3), 507-520.

O'Keefe, B. C. (2008), *Microseismicity of the Central Alpine Fault region, New Zealand:* a thesis submitted to the Victoria University of Wellington in fulfilment of the requirements for the degree of Master of Science in Geophysics, Victoria University of Wellington.

Shi, Y., R. Allis, and F. Davey (1996), Thermal modeling of the Southern Alps, New Zealand, *Pure and Applied Geophysics*, *146*(3-4), X4-500.

Sutherland, R. et al. (2007), Do great earthquakes quakes occur on the Alpine Fault in the central South Island, new Zealand? 235-251. In: Okaya, D.A.; Stern, T.A.; Davey, F.J. (eds) *A continental plate boundary: tectonics at South Island, New Zealand.* Washington, DC: American Geophysical Union. Geophysical monograph 175.

Thurber,C., H.Zhang, T.Brocher, and V.Langenheim, 2009. Regional three-dimensional seismic velocity model of the crust and uppermost mantle of northern California. J.Geophys.Res., 144, doi:10.1029/2008JB005766.

Townend, J. (1999), Heat flow through the West Coast, South Island, New Zealand, *New Zealand Journal of Geology and Geophysics*, *42*(1), 21-31.

Toy, V. G., D. Craw, A. F. Cooper, and R. J. Norris (2010), Thermal regime in the central Alpine Fault zone, New Zealand: Constraints from microstructures, biotite chemistry and fluid inclusion data, *Tectonophysics*, *485*(1-4), 178-192.

Van Avendonk, H. J. A., W. S. Holbrook, D. Okaya, J. K. Austin, F. Davey, and T. Stern (2004), Continental crust under compression: A seismic refraction study of South Island Geophysical Transect I, South Island, New Zealand, Journal of Geophysical Research B: Solid Earth, 109(6), B06302 06301-06316.

Walcott, R. I. (1998), Modes of oblique compression: Late cenozoic tectonics of the South Island of New Zealand, *Reviews of Geophysics*, *36*(1), 1-26.

Waldhauser, F., and W.L.Ellsworth., (2000). A double-difference earthquake location algorithm: Method and application to the northern Hayward fault, California, *Bull. Seismol. Soc. Am.*, 90, 1353-1368.

Wannamaker, P.E., Jiracek, G.R., Stodt, J.A., Caldwell, T.G., Gonzalez, V.M., McKinght, J.D., and Porter, A.D. (2002). Fluid generation and pathways beneath an active compressional orogen, the New Zealand Southern Alps, inferred from magnetotelluric data. *J.Geophys.Res.*, 107, ETG 6, 1-22.

Wannamaker, P.E., T.G. Caldwell, G.R. Jiracek, V. Maris, G.J. Hill, Y. Ogawa, H.M. Bibby, S.L. Bennie, and W. Heise (2009). Fluid and deformation regime of an advancing subduction system at Marlborough, New Zealand. *Nature*, 460, 733-736, doi:10.1038/nature08204

Wellman, H. W. (1979), An uplift map for the South Island of New Zealand, and a model for uplift of the Southern Alps, Bulletin - Royal Society of New Zealand (18), 13-20.

Zhang, H.J., and C.H.Thurber. (2003). Double-difference tomography: The method and its application to the Hayward fault, California, Bull. Seismolo. Soc. Am., 93, 1875-1889.

Acknowledgements

Our thanks go to Department of Conservation staff from the West Coast Conservancy office in Hokitika that facilitated consent for helicopter work within the DOC estate and to GeoNet staff who assisted with the collation and processing of the seismological data. Helicopter support for the MT survey was supplied by Alpine Springs Helicopters and expertly piloted by Bill Hales and who played a key role in the successful execution of the MT field work. Discussions with Susan Ellis and Phaedra Upton are also gratefully acknowledged.